Fluctuations in electron cyclotron resonance plasma in a divergent magnetic field

Sudeep Bhattacharjee, Åshild Fredriksen, and Sayan Chandra

Citation: Physics of Plasmas **23**, 022109 (2016); doi: 10.1063/1.4941595
View online: http://dx.doi.org/10.1063/1.4941595
View Table of Contents: http://aip.scitation.org/toc/php/23/2
Published by the American Institute of Physics

Fluctuations in electron cyclotron resonance plasma in a divergent magnetic field

Sudeep Bhattacharjee,[1] Åshild Fredriksen,[2] and Sayan Chandra[3]
[1]Department of Physics, Indian Institute of Technology—Kanpur, Kanpur 208016, India
[2]Department of Physics and Technology, University of Tromsø—The Arctic University of Norway, N-9037 Tromsø, Norway
[3]Centre Énergie, Matériaux et Télécommunications, Institut national de la recherche scientifique (INRS), 1650 Boul. Lionel Boulet, Varennes, Quebec J3X 1S2, Canada

(Received 7 October 2015; accepted 27 January 2016; published online 17 February 2016)

The dependence of fluctuations on electron-neutral collision frequency (ν_{en}) and the radial location is investigated in an electron cyclotron resonance plasma in a divergent magnetic field region for a set of magnetic fields. Results indicate that the fluctuations depend strongly on the collision frequency. At lower magnetic fields and ν_{en}, the fluctuation levels are small and are observed to peak around 3–5 cm from the central plasma region. Coherent wave modes are found to contribute up to about 30% of the total fluctuation power, and two to three harmonics are present in the power spectra. There are two principal modes present in the discharge: one appears to be a dissipative mode associated with a collisional drift wave instability initiated at a lower pressure (collision frequencies) ($\sim$0.5 mTorr) and is stabilized at a higher pressure ($\gtrsim$3 mTorr). The other mode appears at intermediate pressure ($\gtrsim$1.75 mTorr) and possesses the signature of a flute instability. The fluctuation levels indicate that flute modes are predominant in the discharge at higher pressures ($>$1.75 mTorr) and at higher values of the magnetic field ($\sim$540 Gauss). © *2016 AIP Publishing LLC*.
[http://dx.doi.org/10.1063/1.4941595]

I. INTRODUCTION

Microwave generated electron cyclotron resonance (ECR) plasmas belong to an active area of research, because such plasmas find wide application in several areas of science and technology such as ion sources,[1,2] plasma processing,[3] plasma thrusters for space propulsion,[4,5] and thin films.[6,7]

Conventionally, in ECR plasma devices, research has been primarily focused upon the application in question namely, characterization of the plasma by determination of electron and ion temperatures, particle densities and fluxes on a substrate, and their dependence on external control parameters like gas pressure and microwave power. However, limited attention has been paid to inherent wave modes and instabilities of more interest to the basic plasma physics.

Pool[8] observed transitional instabilities in a nitrogen plasma going from underdense to overdense plasma modes in the pressure range of 0.9 to 1.6 mTorr. The coexistence between the drift and flute wave instabilities in a linear ECR plasma has been studied with an axially imposed boundary.[9] Shoyama *et al.*[10] found intense coherent fluctuations in the ion saturation current when a negative bias was applied to a hollow cathode target in an ECR plasma. Later, low-frequency fluctuations in an ECR plasma source have been investigated with respect to stabilization by localized, radial electric fields by means of a biased, segmented end plate.[11]

In this work, we present the results from an experimental study of fluctuations in the ECR device "Menja" at the University of Tromso, Norway, aimed at understanding the nature of the plasma fluctuations with regard to variations in the external control parameters such as the neutral pressure governing ν_{en} and the electron cyclotron frequency. The region of interest in our experiments is the divergent field region where axial flows of the plasma may be expected because of the gradient in the field and which is away from the upstream region, where the plasma is produced by the ECR mechanism.

Mean values of the floating potential V_f and ion saturation current I_s^+ were obtained at a fixed position for a wide range of the imposed parameters. The fluctuation levels (standard deviation) of V_f over electron temperature T_e as well as relative fluctuation levels of I_s^+ were measured. In addition, radial profiles were obtained for a subset of these. Frequency spectra of time series were analyzed to determine the frequency and power spectra of the fluctuations, and correlation analysis was carried out to investigate the phase shift between the density and potential fluctuations.

Results indicate that at higher pressures ($>$1.32 mTorr) and for larger values of magnetic fields ($>$500 G), the fluctuations in the floating potential are much larger than in the plasma density, a possible indication of flute modes. On the other hand, while the plasma density fluctuations level tends to be low in nearly all parameters, the fluctuation levels of V_f (normalized to T_e) show a much larger variation. The spectra show that a large part of the fluctuations are due to coherent wave modes at low pressures and high magnetic fields, while at higher pressures, the coherent modes are strongly damped. The coherent modes are global modes that do not change much in frequency with radial position, but in the potential and density gradients outside the source cross-section, the modes are driven turbulent. In situations with large coherent modes, several harmonics are found to be present.

The article is organized as follows. In Section II, the experimental set up and measurement is described. In Section III, the results are presented and discussed, and in

Section IV, the results have been summarized and conclusions drawn.

II. EXPERIMENTAL SET-UP AND MEASUREMENT

The schematic of the ECR plasma experimental system is shown in Fig. 1(a). The device has been described in detail earlier by Aanesland and Fredriksen.[12] Two sets of four coils each provide a divergent magnetic field configuration with a maximum close to a conflat flange (CF) port with a quartz window, while another coil placed downstream reduces the magnetic field divergence and improves plasma confinement in the position of the probe diagnostics. The plasma is produced by launching microwaves from a magnetron operating at 2.45 GHz with variable input power in the range 0.5–5 kW through a rectangular wave guide. Data presented in this paper were obtained with microwave power at 500 W. As shown in Fig. 1(b), the ECR magnetic field of 875 G is satisfied in the region between +2 and +20 cm from the quartz window, depending on the applied coil current, where origin is chosen at the position of the window. The change of magnetic field profiles with coil currents is shown in Fig. 1(b).

H_2 is used as the test gas, with flow varied in the range of 1.0–10 sccm (~0.38–4.54 mTorr) and is controlled using a mass flow controller. The coil current is varied from 220 to 270 A, which corresponds to a magnetic field variation of 480–580 G at a radial probe located about 30 cm from the microwave window (cf. Fig. 1(b)). Because of ECR action, the plasma is mainly produced in the neck region indicated by resonance zone in Fig. 1(a) and then flows along the magnetic field lines to the expansion region having a divergent magnetic field.

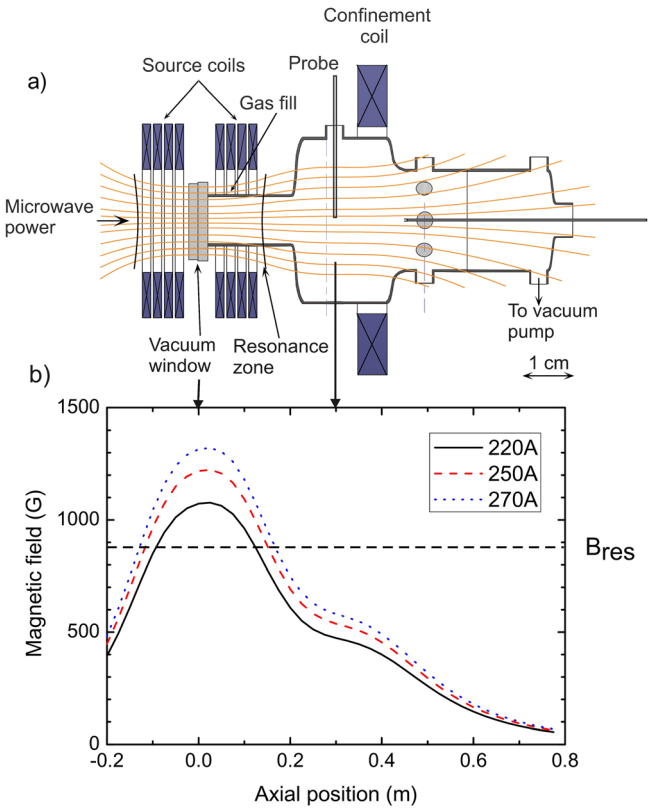

FIG. 1. (a) A schematic drawing of the ECR device. Note the divergent field region where measurements are made (~30 cm from the vacuum window). (b) Axial magnetic field shown for coil currents at 220 A, 250 A, and 270 A.

The experimental variables in the present experiments are discharge pressure and the magnetic field (coil current). Data are obtained by scanning pressure and coil current with the probe placed in the center of the cylindrical cross-section as shown in Fig. 1(a). In addition, radial scans are taken at several of the control parameters mentioned above. Electrostatic cylindrical pin probes are inserted in the downstream region 30 cm from the microwave window as shown in Fig. 1(a) for the measurement of the plasma fluctuations in the floating potential and the ion saturation current. The three cylindrical probe tips (~0.2 mm in diameter and 2 mm long) are made of tungsten. The probes are used to measure the plasma floating potential (V_f) and the ion saturation current (I_s^+). For the V_f measurements, two of the probe pins are floated, and for the I_s^+, the third probe pin is biased at a deep negative potential (~−70 V). The two identical floating probes placed on opposite sides of the biased probe pin helped us to compare nearby local floating potential values and are labeled as Vf_1 and Vf_2. The Vf_2 data will be shown only in some of the plots (e.g., Fig. 3) to provide comparison of results obtained from the two probes pins. The probe for measuring I_s^+ is also used in the Langmuir probe mode (sweep voltage mode) to obtain the probe characteristics for determining the plasma density and the electron temperature.

For Langmuir probe diagnostics, digital I-V scans are obtained from −25 V to +25 V with additional bias provided by a few (1–5) 9 V batteries and in 500 steps of 0.01 V each. Each current data point is averaged 200 times before storing to disk together with the probe bias value. The plasma density is calculated from the electron saturation current at V_p, with the classical formula, where the magnetization of the electrons has been considered by projecting the probe area onto planes perpendicular to the magnetic field,[13] $N_e = 4[I(V_p) - I^+(V_p)]/(A_m v_e q_e)$, where $v_e = \sqrt{8T_e q_e/(\pi m)}$, A_m is the "magnetized" probe area, and $I^+(V_p)$ is the (line fitted) ion current at V_p.

For fluctuation measurements, I_s^+ and V_f are obtained from separate probe pins on a three- (or two-) pin Langmuir probe, and the standard deviations I^+_{std} and $V_{f,std}$ are derived from the fluctuating component of the signals. Time series of 1×10^5 points and for some series, 5×10^5 points at 1 MHz sampling frequency are obtained to yield 0.1 s long data sets with frequency resolution up to 2 Hz and 500 kHz bandwidth. Averaged frequency spectra are computed by dividing the time series in 32 different sub-records about 2000 samples each and computing the FFT of each, resulting in a frequency resolution of 64 Hz. The averages of the 32 spectra are then computed, and spectra shown in Section III are all averaged.

Cross-phase analysis between the ion current and floating potential fluctuations is carried out applying the normalized product of the Fourier series denoted by F[14]

$$\phi(\omega_j)_{1,2} = \tan^{-1}\left(\mathrm{Im}(R_j)/\mathrm{Re}(R_j)\right),$$
$$R = \left[\frac{F^*\left(I^+_{std}(t)\right)F\left(V_{f,std}(t)\right)_{1,2}}{|F\left(I^+_{std}(t)\right)||F\left(V_{f,std}(t)\right)_{1,2}|}\right]. \quad (1)$$

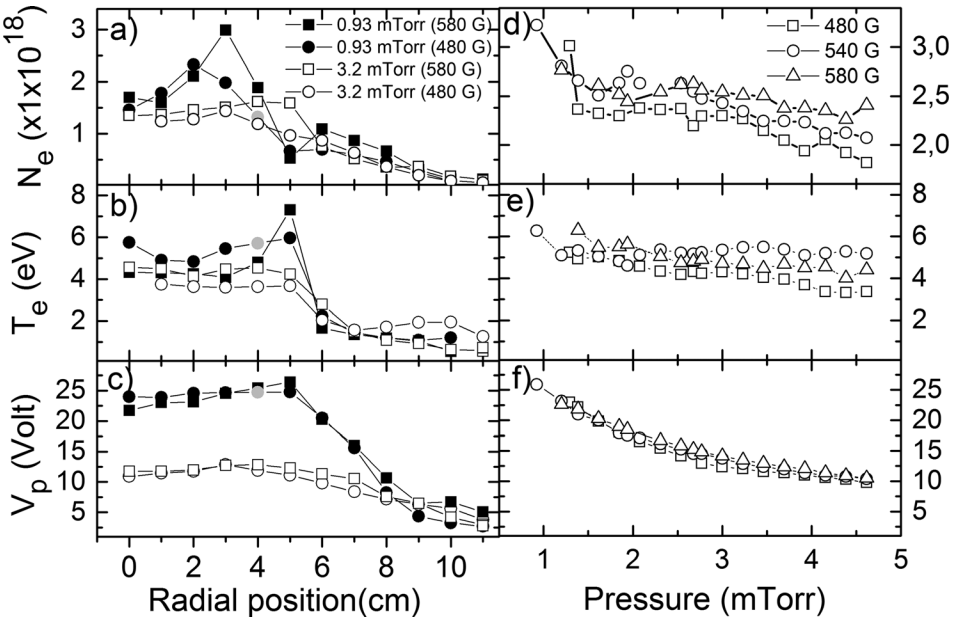

FIG. 2. In the left column are shown the variation of (a) electron density, N_e, (b) electron temperature, T_e, and (c) plasma potential, V_p with radius, at p = 3.2 mTorr and 0.93 mTorr, at 500 W forward microwave power and two magnetic fields (480 G and 580 G at the probe). The 480 G, 0.93 mTorr profile has a missing data point at 4 cm. The grayed points at 4 cm have been obtained from interpolation. The variation of the (d) electron density, (e) electron temperature, and (f) plasma potential with pressure is shown in the right column.

Here, the index j denotes the j'th element of the normalized cross-correlation $R(\omega)$, the indices 1 and 2 imply the 1st and 2nd channel of $V_{f,std}$, and F^* means the complex conjugate of F. To eliminate possible phase displacements due to the spatial offsets between the $V_{f,std}$ and I^+_{std} probe pins, the average of the two different cross-phases is subsequently computed after the frequency average is taken, as described above.

III. RESULTS AND DISCUSSION

A. Background plasma parameters

In Fig. 2 are shown background plasma parameters as derived from Langmuir probe analysis, at high and low magnetic fields (580 G and 480 G, respectively) and at two different pressures, at 0.93 mTorr and 3.2 mTorr. The radial density profiles are shown in Fig. 2(a). At low pressure (0.93 mTorr), they tend to have a peak at 3 cm from the center, where the peak at high magnetic field is most pronounced. These features are followed by a dip at 5 cm. The profiles might be a direct image of the radial position of the microwave deposition in the source; at low collisionality, the ions undergo few collisions until they reach the probe and hence the density profile is not changed much from the source region. At higher magnetic field, the resonance region is pushed outwards toward the main chamber and hence the profile is better retained. At higher pressure, the ions suffer more collisions between the resonance region and the probe, and hence the source profiles show no peaks and only a smooth gradient towards smaller densities outside the source radius of 5 cm, although the density at high magnetic field has a larger gradient.

Figure 2(b) shows the radial variation of the electron temperature (T_e). It is seen that the gradient is maximum between 5 and 6 cm, where the density starts to decrease with increasing distance from center. At low pressures, the temperature has a peaked maximum at the same radial position (5 cm) as the source walls, extending axially up to 20 cm from the microwave window. On the other hand, the temperature is quite uniform at higher pressures until it drops off outside the source radius.

Figure 2(c) shows the radial variation of the plasma potential (V_p) at $p = 3.2$ mTorr and 0.93 mTorr. It can be seen that V_p is almost uniform from the center until a distance of 5 cm, beyond which it drops sharply. The local gradient in V_p is maximum around 5–8 cm. N_e, T_e, and V_p decrease uniformly with pressure as shown in Figures 2(d)–2(f).

Other typical plasma parameters from the Langmuir probe analysis are shown in Table I.

B. Fluctuation measurements

We first tried to identify the fluctuation modes by comparing the ratio of the magnitude of the fluctuations in the floating potential ($V_{f,std}$) to the average values of the electron temperature, given by $V_{f,std}/\langle Te\rangle$, and the ion density ($N_{i\ std}$) to the average value of the plasma (ion) density $N_{i,std}/\langle N_i\rangle$. One of the commonly employed criterion for distinguishing between flute and drift modes is that, if flute

TABLE I. Typical plasma parameters.

Parameter	Typical values
Ion temperature	$T_i \sim 0.5$ eV
Ion neutral collision frequency	$\nu_{in} \sim 3$–15×10^3 Hz at p ~ 0.9–4.5 mTorr
Electron-neutral collision frequency	$\nu_{en} \sim 0.7$–3.5×10^6 Hz at p ~ 0.9–4.5 mTorr
Corresponding mean free paths	$\lambda_{in} \sim 4$–20 cm, $\lambda_{en} \sim 20$–100 cm
Electron-ion mean free paths	$\lambda_{ei} \sim 13$ cm
Ion cyclotron frequency (H^+)	~0.6–1.2 MHz, at 400–800 G
Electron cyclotron frequency[15]	~1.1–2.2 GHz, at 400–800 G

modes are responsible for the fluctuations, it should be indicated by $V_{p,std}/\langle T_e\rangle \gg N_{i,std}/\langle N_i\rangle$. Here, $V_{p,std}$ is represented by $V_{f,std}$, assuming that the T_e fluctuations are small.

From the radial variation of fluctuations levels shown in Figure 3, it was observed that the potential fluctuation levels normalized to T_e are larger than the relative density fluctuations throughout the radius, except near the edge of the plasma column ~10 cm, where fluctuations were small. This was observed at both high and low pressure at low magnetic field of 480 Gauss. We also observe that while the relative density fluctuations are comparatively low throughout the cross-section, the potential fluctuations are much higher inside the main plasma column and falls off outside it, to levels closer to the density fluctuations. In general, judging by fluctuation levels alone, it appears that the fluctuations are all flute-like, with $V_{f,std}/\langle Te\rangle \gg I^{+}{}_{std}/\langle I_{+}\rangle$,[16] although in some parameter intervals, the levels are more comparable as discussed earlier.

The measurement of fluctuations with varying discharge pressure and magnetic field is shown in Figs. 4(a)–4(c). The fluctuations in the floating potential $V_{f,std}$ are larger than the fluctuations in the ion saturation current $I^{+}{}_{std}$ at all the three magnetic fields. For $p < 1.5$ mTorr, we find that the fluctuations in $V_{f,std}$ and I^{+}_{std} are quite small ~0.1. This clearly indicates that the plasma is most stable at these pressures. However, as the pressure increases above 1.5 mTorr, the V_f fluctuation levels increase sharply at magnetic fields $B \geq 540$ G and reaches a maximum plateau value at around $p = 3.0$ mTorr at both high and low magnetic field, although the gradient and maximum level are less pronounced at low field (Figure 4(a)). In contrast to the potential fluctuations, the density fluctuations stay roughly at similar levels for $p > 1.5$ mTorr.

The highest fluctuation levels (~0.6) of V_f are reached at the highest magnetic field (B = 580 G) and high pressure ($p = 2.7$ mTorr), but at all magnetic fields, the fluctuation levels increase with pressure to a maximum value depending upon the magnetic field. Thus, at high pressures, flute modes definitely become dominant in the discharge.

However, we find that the criterion supporting the demarcation may not be strictly valid in regions where the fluctuations levels are more comparable (5%–10%) as seen in the regions of lower pressures (≲1.5 mTorr) of Fig. 4.[9] Instead, upon further investigation as will be shown later, we find that this pressure region ($p \lesssim 1.5$ mTorr) is dominated by drift waves.

To understand better, further time and frequency domain analysis are carried out as detailed in Section III C.

C. Time domain and spectral features

A subset of a typical signal trace in the time domain is shown in Fig. 5(a), along with a sub-range of the Fourier spectrum in Fig. 5(b). The signal has a strong, nearly coherent low-frequency component along with several harmonic

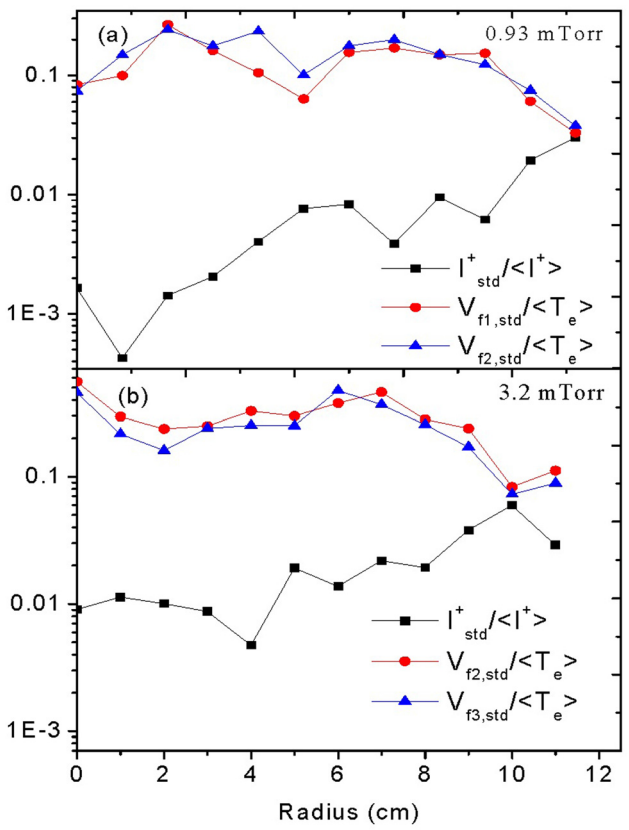

FIG. 3. Radial dependence of fluctuation levels at 500 W and 480 G at a pressure of (a) 0.92 mTorr and (b) 3.2 mTorr.

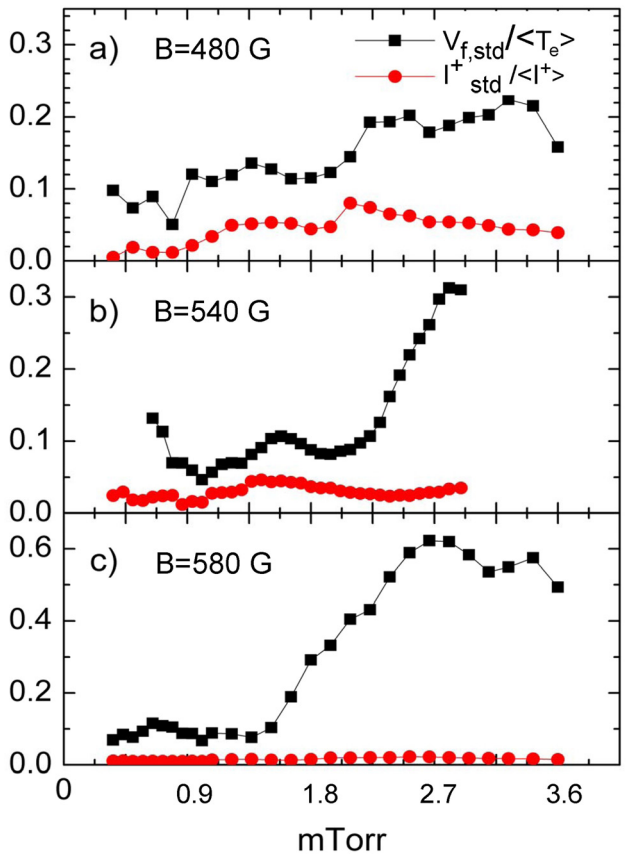

FIG. 4. (a)–(c) Graphs show the relative fluctuations of floating potential and ion saturation current with pressure and for three different magnetic fields (a) 480 G, (b) 540 G, and (c) 580 G. The forward power is kept fixed at 500 W and the reverse power is 25 W for all cases.

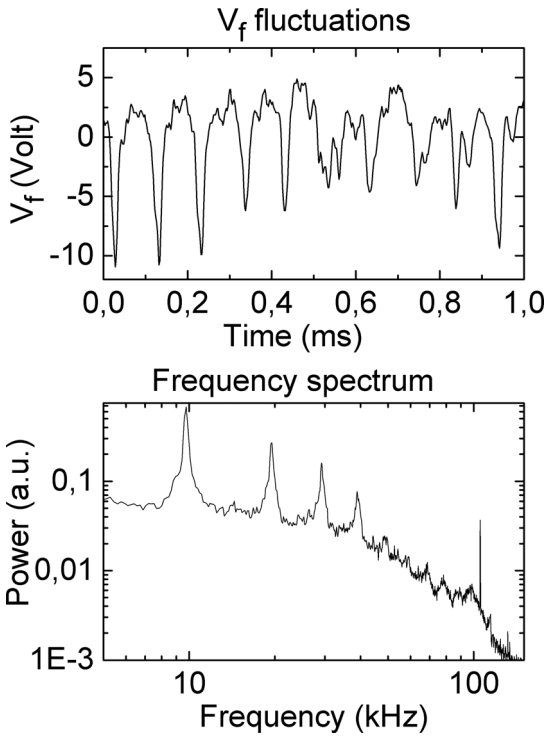

FIG. 5. (a) Typical time series and (b) normalized frequency spectrum, 4 cm outside center of cross section for 3.2 mTorr pressure and B = 580 Gauss. Note that only a part of the total time series is displayed in (a), and the frequency axis in the plot (b) is terminated at 130 kHz, while the maximum frequency range of the spectra is 500 kHz.

components, which is common for a wide range of plasma parameters. The signal power is down by three decades at 100 kHz.

In Fig. 6 is shown a plot of the spectra observed in the middle of the chamber cross-section as a function of pressure. From this spectrogram, it is evident that there is one wave mode with a base frequency starting at about 40 kHz at the lowest pressure of 0.6 mTorr and decreasing with increasing pressure to about 5 kHz at 3.6 mTorr. Another wave mode appears within a pressure range of 1.75–3.5 mTorr. The base mode appears at 1.75 mTorr at about 19 kHz but is visible only within a short pressure range. The strongest component of this wave mode is apparently its 1st harmonic with an onset from the same pressure at about 37 kHz. Its frequency is weakly increasing with pressure until it reaches a plateau around 50 kHz at 3 mTorr. In the following, the two different modes will be named the "Falling Frequency (FF)" mode and the "Rising Frequency (RiF)" mode, respectively.

Clearly, these are two quite different, low-frequency wave modes, of which only the latter one appears to be a flute mode. The drift waves, which are dissipative modes are greatly affected by the discharge pressure, seem to be arising at lower pressures.

Looking at the radial dependence of the modes at the highest pressure of 3.6 mTorr, as shown in Fig. 7, it is seen that the lower frequency component (~7–8 kHz) is more intense and extends over the entire radial distance, indicating a global mode. The 1st harmonic at 15 kHz of the lower frequency appears more pronounced around 6–8 cm. In addition, also the 2nd and 3rd harmonics can be discerned in the region of the density gradients. There is also one more mode around 12 kHz, which extends over the radial location of the density gradient.

The wave amplitude is strongest at ~4.5–7.5 cm. At maximum potential and temperature gradient (see Fig. 2), the wave modes become unstable, showing broadening of peaks and higher power near the mode frequencies. It should be pointed out here that the gradients at that position in the electron temperature are about 1 eV/cm, or $\frac{\nabla T_e}{T_e} \sim 0.3\,\mathrm{cm}^{-1}$, the plasma pressure decreases towards the edges at a normalized ratio $\frac{\nabla nT_e}{nT_e} \sim 0.4\,\mathrm{cm}^{-1}$, and the plasma potential has a normalized gradient of about 0.2–1 cm^{-1}.

To obtain a clearest possible picture of the correlation between the density and potential fluctuations of the most important modes, normalized correlation and phase between the $V_{f,std}$ and I^+_{std} signals (representing potential and density fluctuations, respectively) of the modes were obtained as given in Eq. (1).

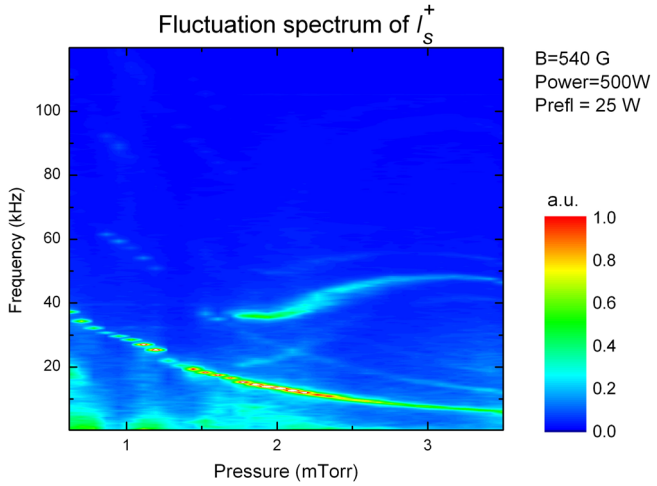

FIG. 6. Spectrogram of fluctuations in the ion saturation current I^+_{std} as a function of pressure with 540 G at the probe, at the center of the plasma column. The color code reflects the variation in spectral power.

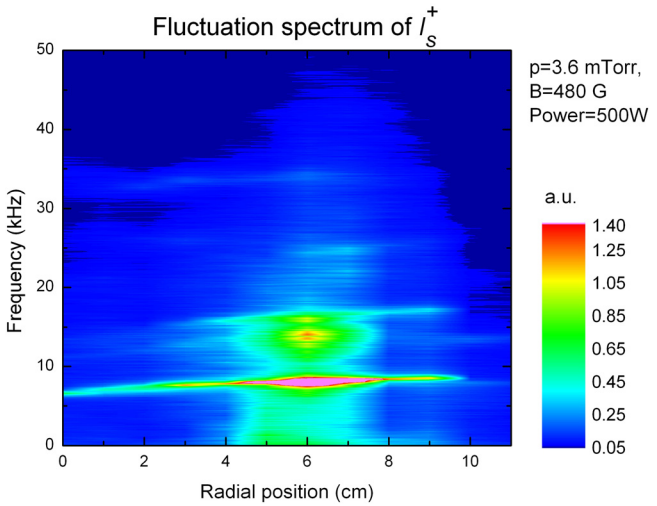

FIG. 7. Radial dependence of modes at 480 G and 3.6 mTorr.

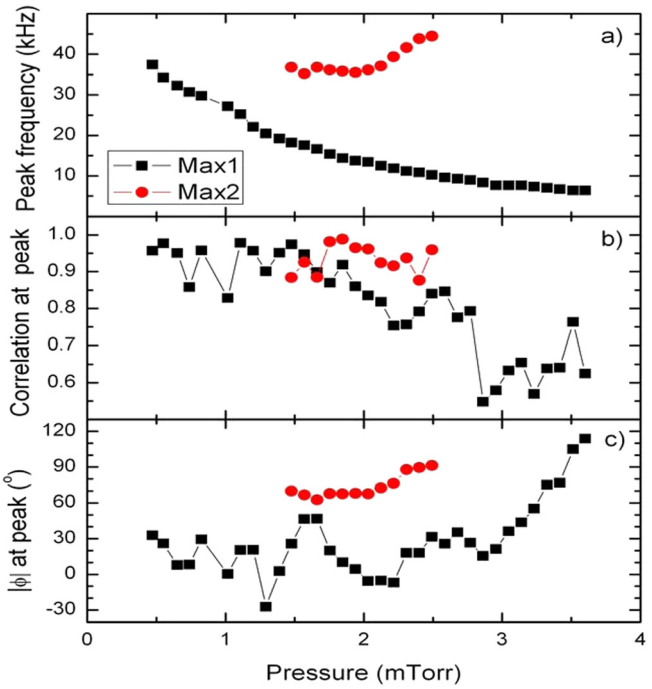

FIG. 8. Frequency of first harmonic peaks in spectrum (a), normalized cross-correlations (b), and absolute phase (c) at peaks. The red (round) symbols belong to the second wave mode appearing at about 1.5 mTorr. As the spectral power of this wave mode decreases with increasing pressures, the values were calculated for a limited pressure range only.

In Figure 8(a) is shown the development of the frequency of the two most important modes with pressure, for the same data set as of Fig. 6.

Normalized correlations between the density and potential at five frequency points centered at the peaks are shown in Figure 8(b), and the absolute value of phase between them is displayed in Figure 8(c). From Figure 8(b), it is evident that the correlation drops off at about 2.8 mTorr for the most prevalent mode. The second mode, appearing at 1.7 mTorr, is too weak for a reliable analysis to be carried out above 2.5 mTorr. Hence, only the larger amplitude part between these pressures is analyzed and showed large normalized correlation throughout this pressure region. The cross-phase between density and potential in this mode is close to $\pi/2$. The phase of the first mode varies between $\pm\pi/6$ for pressures where the correlation is high. None of these phase dependencies are in good agreement with flute modes as indicated from the fluctuation levels analyzed earlier, and it is conjectured that drift waves are a possibility at a lower pressure. The cross-phase for flute modes as reported in Ref. 9 lies in the range $\sim\pi/4$ to $\pi/2$ and is in agreement with the phase of the second wave Max 2 as shown in Fig. 8, as it is seen to lie in this range. Hence, it may be said that the second wave mode is a flute wave. In a toroidal magnetic field, the phase is known to be π for stable flute modes and decreases to $\pi/2$ only for the most unstable modes.[17]

The criterion for exciting flute modes is that the magnetic field radius-of curvature vector $\vec{R}_o$ should be directed away from the region of maximum plasma pressure. In other words, the flute instability occurs only if $\vec{R}_o$ and $\vec{\nabla}p$ are oppositely directed, where R_o is the magnetic field radius of curvature. In the region where the measurements are made, i.e., 30 cm downstream from the microwave window, the flute mode could be excited (cf. Fig. 1, for probe location and direction of field lines), because here the magnetic field lines just start diverging out which implies R_o points towards the plasma column and $\vec{\nabla}p$ of course points away. Therefore, going downstream 30 cm and beyond the microwave window, the flute mode excitation conditions are always met. The flute modes are stable for $2L_n < R_o$, where $L_n = -n/(\partial n/\partial r)$ is the density scale length, positive r is in the radial direction. The radius of curvature $R_o \sim B/|\vec{\nabla}B|$ is of the order of 0.3 to 0.7 m in the radial region between 6 and 10 cm. In our plasma, this criterion is not met within the density gradient for R_o between 6 and 10 cm, as $2L_n$ is larger here than R_o in most of the region of the measurements (typically, $L_n = 28$ cm), and so the possible flute modes in the gradient region do not meet the stability criterion and could have a cross phase different from π.

As of drift modes, their cross-phase would vary between 0 in the adiabatic limit and increase up to $\pi/4$ in the collisional, hydrodynamic limit. The cross-phase of the most prevalent mode, referred to as Max1 in Figure 8, is seen to be within these limits, and thus, this mode could be identified as a drift mode.

The drift wave instability is excited when the ion neutral collisions ν_{in} is low but is stabilized when ν_{in} is high. The drift instability is a global low frequency instability driven by the free energy provided by a pressure gradient transverse to the magnetic field and is sometimes referred to as the dissipative instability.[18] Drift waves have a frequency $\omega^* = k_y v_D$,[19] where v_D is the diamagnetic drift in the direction of k_y. The lowest azimuthal mode at $r = 7$ cm (in the middle of the potential gradient) corresponds to $k_y = 1/(2\pi r) \gg 0.02\,\mathrm{cm}^{-1}$. The flute instability on the other hand comes from the magnetic curvature and is a reactive instability. Ion neutral collisions are therefore important in our plasmas as shown in Table I, with the ion neutral mean free path ($\lambda_{in} \sim 4$–20 cm) being smaller than the electron neutral ($\lambda_{en} \sim 20$–100 cm) and electron ion ($\lambda_{ei} \sim 13$ cm) mean free paths.[20]

From the profiles of the plasma parameters (Fig. 2), the radial electric field E_r in the region of the maximum space potential gradient is $\sim 5\,\mathrm{V\,cm}^{-1}$ at $p = 0.9$ mTorr, and thus the $E \times B$ drift velocity $v_{E\times B}$ is $\sim 1 \times 10^6$ cm s^{-1} for a magnetic field of $B = 515$ G. The electron diamagnetic drift velocity $v_{De} \sim 3 \times 10^5\,\mathrm{cm\,s}^{-1}$ at the same radial location ($r = 7$ cm), which is given by $v_{De} = (\kappa T_e/eB) \times (1/n)(dn/dr)$. As both T_e and the density gradient decrease with pressure (Fig. 2), v_{De} and ω^* decrease with pressure. Both $v_{E\times B}$ and v_{De} have the same direction. It is noted that the frequency corresponding to the diamagnetic drift $f_{De} = (m/r)(\mathbf{v}_{De}/2\pi)$ is around 25 KHz at the location of the steepest density gradient ($r = 5$ cm and 0.9 mTorr), decreasing to about 9 kHz at 3.2 mTorr, which is close to what is observed experimentally in the FF mode.

The $E \times B$ drift corresponds to a frequency $f_{E\times B} = (m/r)(\mathbf{v}_{E\times B}/2\pi) \sim 25$–60 KHz (for azimuthal wave number $m \sim 1$–3, $r = 7$ cm), decreasing at high pressure and the same radius to about 3.5–10 kHz. Thus, the $E \times B$ drift and

the diamagnetic drift give rise to comparable drifts, and the combination of the two could well enhance the harmonics seen in the spectra.

It is interesting to note from Fig. 6 that the RiF mode appears at the pressure where the two modes have the same frequency (~1.5 mTorr), and corresponding to the $E \times B$ drift at this pressure. (As the f_{ExB} was derived at a lower pressure of 0.9 mTorr, the E-field and thus f_{ExB} is expected to be slightly less at 1.5 mTorr). At the given pressure of ~1 mTorr, it corresponds to the observed 1st harmonics of the strongest modes observed.

IV. SUMMARY AND CONCLUSIONS

From the above study, we can generalize a few observations regarding the plasma fluctuations in V_f and I_s. The fluctuations are always higher at a higher pressure, which in our experiment is ~2.5 mTorr and beyond. From the radial studies, we learn that the fluctuations peak around 4–5 cm for the floating potential and around 4–6 cm for the ion saturation current. The radial peaks in fluctuations are induced by the gradients in the plasma potential, the electron temperature, and plasma density. In the boundary plasma ($r = 10$–12 cm), it is observed that the difference in the relative magnitude of fluctuations in the floating potential and the plasma density is comparable. With increasing pressure, the fluctuations increase at the center. Fluctuations in floating potential are larger than the fluctuations in the ion saturation current for all cases indicating that the flute modes are dominant. The fluctuation spectrum, however, indicates that there is one wave mode at a lower pressure (~40 kHz), decreasing in frequency with increasing pressure to ~5 kHz at 3.6 mTorr, which may indicate a drift wave and agreeing with calculations of the $E \times B$ drift. From about 1.75 mTorr, another new wave mode appears with its frequency weakly increasing with pressure ~37 kHz at 1.75 mTorr to ~50 kHz at 3 mTorr. This mode appears to be a flute wave. The radial variation of the modes indicates that these are global modes, particularly the ones at lower frequency. The amplitude of the modes is strongest near 4.5–7.5 cm where the gradients are the largest.

ACKNOWLEDGMENTS

One of the authors (S.B.) gratefully acknowledges financial support from a Norwegian Government Scholarship of the Norwegian Research Council for specialist exchange in December 2006, under the cultural agreement between Norway and India, which has made this research work possible. S.B. extends sincere thanks to Prof. A. Fredriksen for the warm hospitality and for partial travel support in this collaborative work. We thank Prof. Hans Pécseli for helpful comments.

[1]H. Ito, S. Ito, M. Tahashi, N. Sakudo, A. Kawasaki, and N. Ikenaga, Int. Conf. Ion Implant. Technol. Proc. **1**, 558 (1999).
[2]Y. Matsubara, H. Tahara, M. Takahashi, and S. Nogawa, Rev. Sci. Instrum. **63**, 2595 (1992).
[3]T. H. Chang, L. R. Barnett, K. R. Chu, F. Tai, and C. L. Hsu, Rev. Sci. Instrum. **70**, 1530 (1999).
[4]Y. Juan, H. Hongqing, and H. Xianwei, J. Spacecr. Rockets **41**, 126 (2004).
[5]M. A. Kemp and S. D. Kovaleski, J. Appl. Phys. **100**, 113306 (2006).
[6]A. Yanguas-Gil, J. Cotrino, and A. R. González-Elipe, J. Phys. D: Appl. Phys. **40**, 3411 (2007).
[7]S. Nakayama, Pure Appl. Chem **62**, 175 (1990).
[8]S. Pool, J. Appl. Phys. **81**, 2839 (1997).
[9]K. Kamataki, Y. Nagashima, S. Shinohara, Y. Kawai, M. Yagi, K. Itoh, and S. I. Itoh, J. Phys. Soc. Jpn. **76**, 054501 (2007).
[10]H. Shoyama, M. Misina, and S. Mitake, Jpn. J. Appl. Phys., Part 1 **36**, 4583 (1997).
[11]M. Yoshinuma, M. Inutake, R. Hatakeyama, T. Kaneko, K. Hattori, A. Ando, and N. Sato, Phys. Lett. A **255**, 301 (1999).
[12]A. Aanesland and A. Fredriksen, J. Vac. Sci. Technol. A **19**, 2446 (2001).
[13]I. H. Hutchinson, *Principles of Plasma Diagnostics* (Cambridge University Press, Cambridge, 1987).
[14]M. Koga and Y. Kawai, Phys. Plasmas **10**, 650 (2003).
[15]M. A. Lieberman and A. J. Lichtenberg, *Principles of Plasma Discharges and Materials Processing* (Wiley & Sons, Hoboken, NJ, 2005).
[16]E. J. Powers, Nucl. Fusion **14**, 749 (1974).
[17]O. E. Garcia, J. Plasma Phys. **65**, 81 (2001).
[18]A. V. Timofeev and B. N. Shvilkin, Sov. Phys. Usp. **19**, 149 (1976).
[19]T. Mikkelsen and H. L. Pécseli, Phys. Lett. **77A**, 159 (1980).
[20]K. Kamataki, S.-I. Itoh, Y. Nagashima, S. Inagaki, M. Yagi, T. Yamada, Y. Kawai, A. Fujisawa, and K. Itoh, Plasma Phys. Controlled Fusion **50**, 035011 (2008).